

# The clustering of radio galaxies at $z \simeq 0.55$ from the 2SLAQ LRG survey

David A. Wake<sup>1</sup>, Scott M. Croom<sup>2</sup>, Elaine M. Sadler<sup>2</sup>, Helen M. Johnston<sup>2</sup>

<sup>1</sup>*Department of Physics, University of Durham, South Road, Durham DH1 3LE, UK*

<sup>2</sup>*School of Physics, University of Sydney, NSW 2006, Australia*

## ABSTRACT

We examine the clustering properties of low-power radio galaxies at redshift  $0.4 < z < 0.8$ , using data from the 2SLAQ Luminous Red Galaxy (LRG) survey, and find that radio-detected LRGs (with typical optical luminosities of  $3 - 5 L_*$  and 1.4 GHz radio powers in the range  $10^{24}$  to  $10^{26}$  W Hz<sup>-1</sup>) are significantly more clustered than a matched population of radio-quiet ( $\lesssim 10^{24}$  W Hz<sup>-1</sup>) LRGs with the same distribution in optical luminosity and colour.

The measured scale length of the two-point cross-correlation function between the full LRG sample and the radio-detected LRGs is  $9.57 \pm 0.50 h^{-1}$  Mpc, compared to  $8.47 \pm 0.27 h^{-1}$  Mpc for the matched sample of radio-quiet LRGs; while the implied scale length of the auto-correlation function,  $r_0$ , is  $12.3 \pm 1.2 h^{-1}$  Mpc and  $9.02 \pm 0.52 h^{-1}$  Mpc for the radio-detected and radio-quiet samples respectively. We further interpret our clustering measurements in the halo model framework and demonstrate that the radio-detected LRGs have typical halo masses of  $10.1 \pm 1.4 \times 10^{13} h^{-1} M_\odot$  and bias of  $2.96 \pm 0.17$ , compared to  $6.44 \pm 0.32 \times 10^{13} h^{-1} M_\odot$  and  $2.49 \pm 0.02$  for the radio-quiet sample. A model in which the radio-detected LRGs are almost all central galaxies within haloes provides the best fit to the measured clustering, and we estimate that at least 30% of all 2SLAQ LRGs with the same clustering amplitude as the radio-detected LRGs are currently radio-loud.

Our results imply that radio-detected galaxies in the 2SLAQ LRG sample typically occupy more massive haloes than other LRGs of the same optical luminosity, so the probability of finding a radio-loud AGN in a massive galaxy at  $z \sim 0.55$  is influenced by the halo mass and/or cluster environment in addition to the well-known dependence on optical luminosity. If we model the radio-detected fraction of LRGs,  $F_{\text{rad}}$ , as a function of halo mass  $M$ , then the data are well-fitted by a power law of the form  $F_{\text{rad}} \propto M^{0.65 \pm 0.23}$ . The observed relationship between radio emission and clustering strength could plausibly arise either through a higher fuelling rate of gas onto the central black holes of galaxies in the most massive haloes (producing more powerful radio jets) or through the presence of a denser IGM (which would provide a more efficient working surface for the jets, thus boosting their observed radio luminosity). Further work is needed to determine which of these effects is dominant.

**Key words:** cosmology: observations – galaxies: clusters: general – galaxies: active – radio continuum: galaxies – galaxies: evolution – galaxies: elliptical and lenticular, cD – cosmology: large-scale structure of Universe

## 1 INTRODUCTION

### 1.1 Radio galaxies and their environment

It has long been known that the hosts of powerful radio-loud AGN are massive early-type galaxies, and that the probability of such a galaxy hosting a radio source increases rapidly with optical luminosity and stellar mass (Auremma et al. 1977; Best et al. 2005a; Mauch & Sadler 2007). What re-

mains less clear is the role (if any) of a galaxy’s environment in determining whether it hosts a radio source.

Studies carried out in the 1980s hinted at significant differences between the clustering properties of the powerful FRII<sup>1</sup> radio galaxies and the less powerful FRI sources.

<sup>1</sup> Fanaroff & Riley (1974) divided radio galaxies into two classes based on their observed radio morphology. They found a correla-

Based on an imaging study of 43 radio galaxies at  $z < 0.3$ , Heckman et al. (1986) found that the most powerful radio sources (with radio luminosities above  $10^{25.5} \text{ W Hz}^{-1}$  at 408 MHz) lay in regions of below-average galaxy density and often showed a disturbed morphology suggestive of a recent interaction with a gas-rich companion. In contrast, less powerful radio sources appeared to be associated with morphologically-normal early-type galaxies in regions of high local galaxy density. Similar results were obtained by Prestage & Peacock (1988), who used an angular cross-correlation technique to study the clustering environment of a sample of about 200 nearby ( $z < 0.15$ ) radio galaxies. They found that FRI radio galaxies lay in regions of significantly enhanced galaxy density, whereas the clustering environment of FR II sources was similar to that of the overall population of ‘normal’ elliptical galaxies.

The picture changed significantly in the mid 1990s with the work of Ledlow & Owen (1996), who discovered that the division in radio power between FRI and FR II radio sources was a strong function of the optical luminosity of the host galaxy. As a result, FR II radio sources are generally hosted by less optically luminous (and less massive) galaxies than FRI sources of similar radio power. Since more massive galaxies also tend to be more strongly clustered, this effect needs to be taken carefully into account when analysing the clustering properties of powerful radio sources. Ledlow & Owen (1996) measured the bivariate radio luminosity function (RLF) of early-type galaxies in rich clusters, and found no statistically significant difference between the RLFs of galaxies in rich clusters and in the field. Their results suggested that the local environment plays little or no role in determining whether an early-type galaxy hosts a radio-loud AGN, and that the optical luminosity and other properties of the host galaxy are by far the most important parameters affecting radio source formation and evolution.

## 1.2 Measurements of radio-source clustering

The advent of large galaxy redshift surveys like the 2dFGRS and SDSS (Colless et al. 2001; York et al. 2000), combined with ‘‘all-sky’’ radio continuum surveys like NVSS and SUMSS (Condon et al. 1998; Bock et al. 1999) made it possible to assemble samples of thousands of objects with which to carry out statistical analyses of radio galaxies in the local universe (Best et al. 2005b; Mauch & Sadler 2007). The NVSS and SUMSS source catalogues are large and uniform enough that the characteristic imprint of large-scale structure can easily be seen in the angular correlation function (Blake & Wall 2002; Blake et al. 2004). Convolving the angular clustering amplitude in these surveys with a characteristic redshift distribution  $N(z)$  suggests that the present-day clustering length  $r_0$  of radio galaxies is in the range of 7–10  $h^{-1}$  Mpc, corresponding to a clustering strength similar to optically-luminous elliptical galaxies in moderately rich environments (see e.g. Overzier et al. 2003).

Recently, Best et al. (2007) have revisited the question of radio-source clustering using data sets much larger than

those available to Ledlow & Owen (1996). Using a sample of 625 nearby galaxy groups and clusters selected from the SDSS, they show that the brightest galaxies in groups and clusters (BCGs) are more likely to host a radio-loud AGN than other galaxies of the same stellar mass. The probability is increased by up to a factor of two for the most massive galaxies (with stellar mass  $\sim 5 \times 10^{11} M_{\odot}$ ), and by over an order of magnitude for galaxies with stellar masses below  $10^{11} M_{\odot}$ . This enhanced likelihood of radio-loud AGN activity was only seen in the innermost regions of a group or cluster (i.e. within  $0.2 r_{200}$ , where  $r_{200}$  is the Virial radius of the cluster). Best et al. (2007) argue that the radio properties of both BCGs and non-BCGs can be explained if the radio emission is mainly fuelled by cooling gas from an X-ray halo surrounding the galaxy. It therefore appears that although the radio properties of most galaxies in the local universe are largely unaffected by their environment, this is not true for massive galaxies located in the central regions of clusters.

## 1.3 The 2SLAQ LRG radio sample at $z \sim 0.55$

At higher redshift, Sadler et al. (2007) recently combined data from the 2SLAQ Luminous Red Galaxy (LRG) redshift survey (Cannon et al. 2006) and the NVSS and FIRST radio surveys (Condon et al. 1998; Becker et al. 1995) to identify a volume-limited sample of 391 radio galaxies at redshift  $0.4 < z < 0.7$ . They measured the redshift-space correlation between the radio-detected 2SLAQ LRGs and the full LRG sample, and found that the 2SLAQ radio galaxies were more strongly clustered than the overall 2SLAQ LRG population. Since the 2SLAQ radio galaxies as a class were also more optically luminous than the overall LRG sample it was unclear whether the increased clustering was a luminosity effect, or represented a genuine difference in the environments of radio-loud and radio-quiet LRGs at  $z \sim 0.55$ . In the current paper, our goal is to answer this question by investigating the clustering properties of radio-loud 2SLAQ LRGs in more detail.

## 1.4 Radio-galaxy duty cycles

The inferred lifetimes of the radio sources associated with massive galaxies (typically  $10^6$ – $10^8$  yr; Parma et al. 1999) are significantly shorter than the ages of their parent galaxies, so it is generally assumed that all massive galaxies must cycle between radio-loud and radio-quiet phases over time. Feedback mechanisms in which the hot intergalactic gas episodically cools to fuel a central AGN, and is then reheated by the ensuing radio jets (e.g. Binney & Tabor 2005, Ciotti & Ostriker 2007) provide a natural explanation for this process.

For the 2SLAQ LRG sample, Johnston et al. (2008) have shown that the stellar populations of radio-detected and radio-quiet galaxies are generally indistinguishable. This is consistent with a picture in which ‘radio-mode’ AGN feedback (Bower et al. 2006; Croton et al. 2006) regulates the star-formation rate in these massive galaxies, and all of them undergo radio-loud episodes when their central black hole is active and can power radio jets. If this is the case, then the fraction of galaxies which are detected as radio

tion between morphology and radio luminosity, with less luminous (FRI) sources having a jet-like appearance and more luminous (FR II) sources having edge-brightened radio hotspots.

**Table 1.** Summary of the three 2SLAQ LRG samples used in this clustering study.

Set	Properties	N
1	All ‘Sample 8’ LRGs with good-quality $z$	7009
2	Radio-detected LRGs from Set 1	250
3	Luminosity-matched set of LRGs from Set 1	2750

sources above some radio power  $P_{\text{lim}}$  simply represents the fraction of the radio-galaxy duty cycle for which a typical galaxy is a radio source at or above this level.

Observationally this is complicated by the fact that the radio luminosity function of AGN is very broad, spanning at least six orders of magnitude (Mauch & Sadler 2007), and there is also a strong correlation between radio power and optical luminosity (Auremma et al. 1977, Best et al. 2005). The observed radio detection rate will therefore depend strongly on both radio power and galaxy luminosity. In this paper we consider only the very luminous early-type galaxies which comprise the 2SLAQ LRG sample, so that the range in optical luminosity is small. We also use the term ‘radio-detected’ to refer to galaxies whose 1.4 GHz flux density is higher than the 1–2 mJy detection limit of the FIRST and NVSS radio surveys. Since the 2SLAQ LRG radio sample is close to volume-limited (see Figure 7 of Sadler et al. 2007), this translates to a limiting radio luminosity of  $\sim 10^{24.2} \text{ W Hz}^{-1}$ .

Throughout this paper, we assume a flat  $\Lambda$ -dominated cosmology with  $\Omega_m=0.27$ ,  $H_0=70 \text{ km s}^{-1}\text{Mpc}^{-1}$ , and  $\sigma_8=0.8$  unless otherwise stated.

## 2 THE 2SLAQ LRG DATA SAMPLES

In this paper we will consider the clustering of three data sets, as summarised in Table 1. All three samples are drawn from the full 2SLAQ LRG spectroscopic survey (Cannon et al. 2006). The first data set consists of all main sample (‘Sample 8’) LRGs with high quality redshifts and  $0.45 < z < 0.8$  (see Cannon et al. 2006 for details). The second set is a sub-sample of the first, and includes only the LRGs which have been detected as radio sources (see Sadler et al. 2007). Since we want to test whether radio-detected LRGs are more strongly clustered, we select a further sub-sample which has the same optical properties as the radio-detected sub-sample but does not contain any LRGs with detected radio emission.

Figure 1 shows the distribution of the intrinsic luminosity, redshift and colour of the whole LRG sample and the radio-detected subsample, where we have used the  $K+\epsilon$  corrections as detailed in Wake et al. (2006) to generate the intrinsic luminosity and colours. This figure shows that the radio sample is intrinsically more luminous, has a slightly higher typical redshift and is slightly redder. As a result of this, to generate a matched sample of LRGs without radio emission we must match for both optical luminosity and redshift. To be complete we also match for colour, even though the difference in the distributions is marginal. We note that excluding this colour matching makes no difference to our results. We generate our sample by selecting the eleven LRGs from the whole sample that lie closest to each radio-detected

LRG in colour-magnitude-redshift space. The final matched sample contains 2750 LRGs, which is the maximum that can be generated if we want to match the radio distributions without a large number of repeats ( $\sim 15\%$ ).

## 3 THE TWO-POINT CROSS-CORRELATION FUNCTION

Since the space density of the radio LRG sample is very low, measurements of its auto-correlation function would be dominated by shot noise, particularly on small scales. In order to reduce this noise we cross-correlate the radio and matched samples with the full LRGs sample, which has a much higher space density.

The 2pt-cross-correlation function between two sets of objects  $a$  and  $b$ ,  $\xi_{ab}(r)$ , is defined as a measurement of the excess probability above Poisson of finding an object  $a$  at a separation  $r$  from another object  $b$ . Here we wish to cross-correlate the radio and matched samples with the full LRG sample. We calculate this by comparing the number of pairs as a function of scale between the radio-detected (or matched) and full sample, with the number of pairs between the radio (or matched) and an unclustered (random) catalogue, which covers the same volume as the full sample such that

$$\xi(s) = \frac{n_R N_{Rf}(r)}{n_f N_{Rr}(r)} - 1, \quad (1)$$

where  $N_{Rf}$  and  $N_{Rr}$  are radio-full and radio-random pair counts respectively, and  $n_f$  and  $n_r$  are the number of galaxies in the full and random samples.

When making this calculation for our samples we must take into account the effect of the completeness varying across our survey. We follow the procedure described in detail by Wake et al. (2008), by up-weighting LRGs in areas of low completeness and using a random catalogue that has a constant space density over the angular mask of the survey. We exclude from our calculations regions that have  $< 65\%$  completeness or that are close to bright stars.

We estimate the errors on our 2pt-cross-correlation function measurements using jack-knife re-sampling (Scranton et al. 2002; Zehavi et al. 2005). We split the 2SLAQ area into 74 equal area regions, minimising the noise on the covariance matrix whilst still removing regions larger than the scales we are interested in. We then repeatedly calculate each 2pt-function removing one area at a time to generate a full covariance matrix. Throughout we generate the pair counts using the KD-tree code in the NTROPY software package (Gardener et al. 2007).

The peculiar velocities of galaxies generate an error in the distance measurement to a galaxy along the line of sight, which results in distortions to  $\xi$  known as redshift space distortions. To remove this effect we can calculate the clustering perpendicular ( $r_p$ ) and parallel ( $\pi$ ) to the line-of-sight ( $\xi(r_p, \pi)$ ) and then integrate over the  $\pi$  direction to 80  $h^{-1}\text{Mpc}$  to give the projected correlation function ( $w(r_p)$ ) such that

$$w_p(r_p) = 2 \int_0^\infty d\pi \xi(r_p, \pi). \quad (2)$$

This can be expressed in terms of the real space correlation function  $\xi(r)$  (Davis & Peebles 1983) with

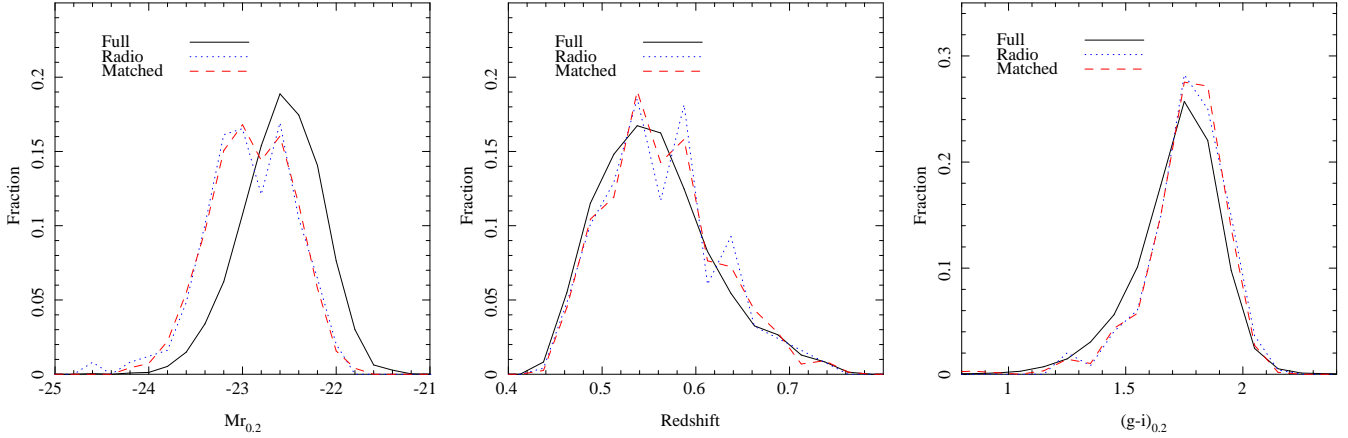


**Figure 1.** The luminosity (left), redshift (middle) and colour (right) distributions of the full LRG sample (solid), the radio sample (dotted) and a sample randomly selected from the whole sample to match the luminosity, colour and  $z$  distributions of the radio sample (dashed).

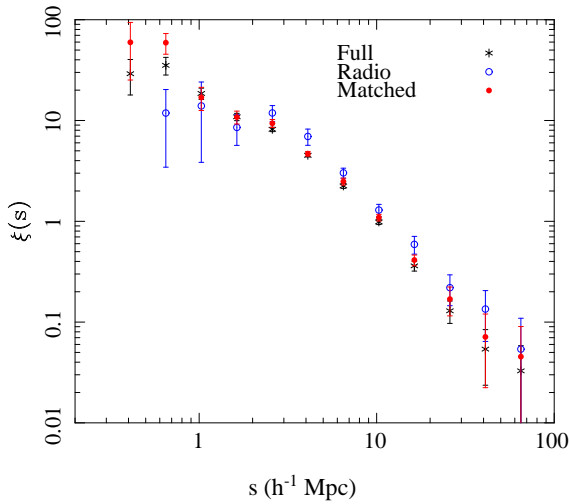


**Figure 2.** The redshift space 2pt-auto-correlation function for the full LRG sample (stars) and the redshift space 2pt-cross-correlation function for the radio sample (open circles) and a sample randomly selected from the whole sample to match the luminosity, colour and redshift distributions of the radio sample (filled circles).

$$w_p(r_p) = 2 \int_{r_p}^{\infty} r dr \xi(r) (r^2 - r_p^2)^{-1/2}. \quad (3)$$

If a power law of the form  $\xi(r) = (r_0/r)^{-\gamma}$  is assumed then equation 3 can be solved analytically (Davis & Peebles 1983).

#### 4 CLUSTERING PROPERTIES OF RADIO-DETECTED LRGs AT $Z \sim 0.55$

Figures 2 and 3 shows the 2pt-auto-correlation function for the full sample, and the 2pt-cross-correlation function for the radio-detected and matched samples in redshift space and

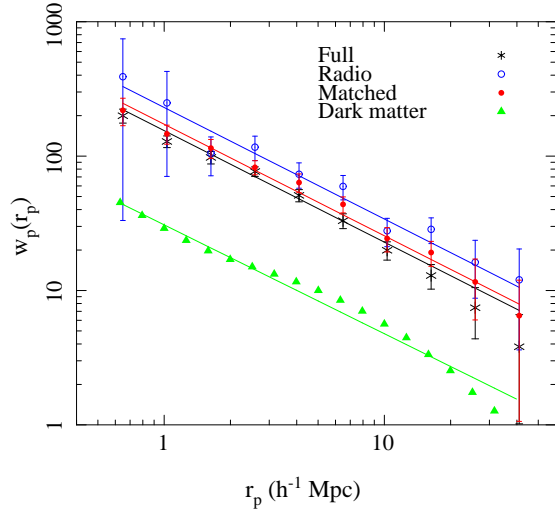


**Figure 3.** The projected 2pt-auto-correlation function for the full LRG sample (stars) and dark matter (triangles), and the 2pt-cross-correlation function for the radio sample (open circles) and a sample randomly selected from the whole sample to match the luminosity, colour and redshift distributions of the radio sample (filled circles). The lines show power-law fits on scales  $0.5 < r_p < 50 h^{-1}$  Mpc with slope,  $\gamma$ , fixed at 1.83 corresponding to the best fit value for the full 2SLAQ LRG sample.

projection respectively. In order to compare the clustering strengths of these samples we make  $\chi^2$  fits to  $w(r_p)$  assuming a power law form for  $\xi(r)$  of  $(r/r_0)^{-\gamma}$  using the analytical solution to equation 3. We use the full covariance matrices generated using the jack-knife resampling technique and fit over  $0.5 < r_p < 50 h^{-1}$  Mpc. Values of  $r_0$  and  $\gamma$  for these fits are given in Table 2. Since the values of the slope,  $\gamma$ , are consistent between the three samples we refit using the  $\gamma$  from the fit to the full LRG sample. The values of  $r_0$  from these fits are also given in Table 2 and the  $\Delta\chi^2$  distributions are shown in Figure 4.

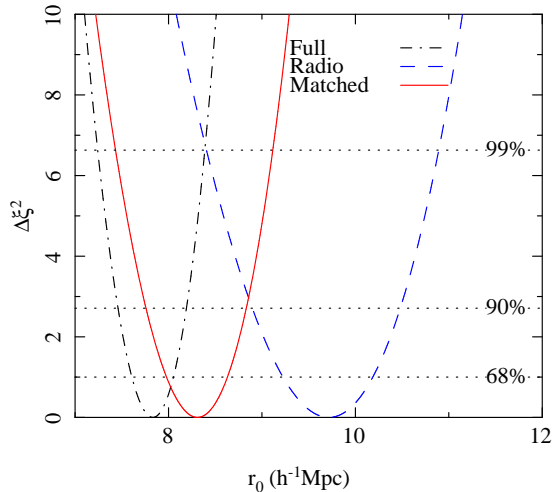


**Figure 4.**  $\Delta\chi^2$  for the power law fits to the projected 2pt-cross-correlation functions for the radio sample (blue dashed), a sample matching the luminosity, colour and redshift distributions of the radio sample (red solid), and the auto-correlation function of the full LRG sample (black dot-dashed). The slope,  $\gamma$ , is fixed at 1.83 corresponding to the best fit value for the full sample. The horizontal dotted lines show the 68%, 90% and 99% confidence intervals.

**Table 2.** Values of the power-law fits to the projected 2pt-auto-correlation function for the full sample and dark matter, and the 2pt-cross-correlation function for the radio and matched samples in the range  $0.5 < r < 50h^{-1}$  Mpc. Errors are at the 68% confidence level.

Sample	$r_0$ ( $h^{-1}$ Mpc)	$\gamma$	$\chi_{red}^2$	$r_0$ (fixed $\gamma$ )
Full	$7.66^{+0.16}_{-0.17}$	$1.83^{+0.04}_{-0.04}$	1.6	$7.66^{+0.16}_{-0.17}$
Matched	$8.47^{+0.27}_{-0.27}$	$1.78^{+0.05}_{-0.05}$	1.4	$8.31^{+0.22}_{-0.23}$
Radio	$9.57^{+0.51}_{-0.50}$	$1.75^{+0.10}_{-0.10}$	1.8	$9.72^{+0.49}_{-0.46}$
Dark Matter	$3.25^{+0.02}_{-0.02}$	$1.81^{+0.02}_{-0.02}$	–	–

Figure 4 and Table 2 show that the radio-detected LRGs are more clustered (with a significance of 97%) than other LRGs with similar optical luminosity. When considering Figures 2, 3 and 4 and the fits given in Table 2, it is important to remember that the amplitude of the cross-correlation of the radio or luminosity matched samples will be lower than the auto-correlation for these samples, since they are cross-correlated with the full LRG sample which has a lower clustering strength. On large ( $> 1$  Mpc) scales, where the clustering is determined by pairs of galaxies in separate dark matter haloes, one would expect the cross-correlation function to be the geometric mean of the auto-correlation of the two samples. On smaller scales where the clustering is dominated by pairs within haloes, the cross-correlation function will depend on the relative distribution of the two samples within haloes and would only be the mean if the distribution was identical. We can therefore use the cross-correlation on large scales to calculate the auto-correlation function, where

**Table 3.** The scale length of 2pt-auto-correlation function ( $r_0$ ) for the three samples along with the inferred large scale bias and typical dark matter halo mass. Errors are at the 68% confidence level.

Sample	$r_0$ ( $h^{-1}$ Mpc)	bias	$M_{DH}(10^{13}h^{-1}M_{\odot})$
Full	$7.66\pm 0.17$	$2.14\pm 0.05$	$3.1\pm 0.2$
Matched	$9.02\pm 0.52$	$2.52\pm 0.16$	$5.7\pm 1.1$
Radio	$12.3\pm 1.2$	$3.11\pm 0.29$	$10.6\pm 1.9$

$$\xi_2 = \xi_{12}^2 / \xi_1. \quad (4)$$

This gives values of  $r_0$  for the auto-correlation function of  $12.3 \pm 1.2$  and  $9.02 \pm 0.52 h^{-1}$  Mpc for the radio-detected and matched samples respectively.

We can estimate the large scale bias ( $b$ ) for our three populations as  $b = (w_{pGal}/w_{pDM})^{1/2}$  where  $w_{pDM}$  is generated using the linear theory power spectrum as described in section 5 and the projected auto-correlation function for the matched and radio-detected samples is calculated using Equation 4. We define the large scale bias here as the weighted mean of  $(w_{pGal}/w_{pDM})^{1/2}$  within  $2 < r < 50 h^{-1}$  Mpc. We can then use the dependence between the dark matter halo mass and bias estimated from the halo mass function (Sheth & Tormen 1999) to relate this bias to a typical halo mass. Table 3 gives the mean bias and halo mass for each of the three samples.

Our finding that the radio-detected 2SLAQ luminous red galaxies (which have typical 1.4 GHz radio powers of  $10^{24}$  to  $10^{26}$   $\text{W Hz}^{-1}$ ) are significantly more strongly-clustered than LRGs of similar optical luminosity which are not detected as radio sources (and so are weaker than  $\sim 10^{24}$   $\text{W Hz}^{-1}$ ) implies that the radio-galaxy duty cycle  $z \sim 0.55$  is affected by at least one factor which is linked to the clustering environment, and we investigate this further in the next section.

## 5 HALO MODELS

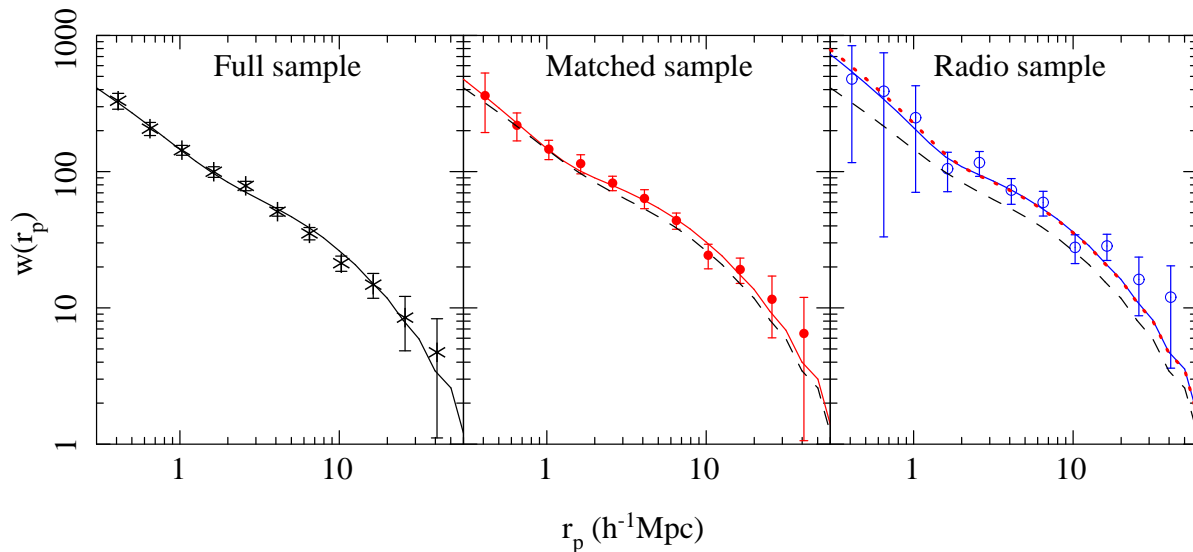
### 5.1 Model parameters

The halo model assumes that the galaxy clustering signal encodes information about the Halo Occupation Distribution (HOD; how the galaxies populate dark matter haloes), in particular how the HOD depends on halo mass (see e.g. Jing et al 1998, Ma & Fry 2000, Peacock & Smith 2000, Seljak 2000, Scoccimarro et al. 2001, Berlind & Weinberg 2002). We have successfully applied this technique to the 2pt-correlation function of the 2SLAQ LRGs (Wake et al. 2008), and use the same techniques here to gain a further understanding of how the radio galaxies are distributed within dark matter haloes. We give below a brief outline of our halo model description of the clustering, and refer the reader to Wake et al. (2008) for further details.

In the halo model, every galaxy is associated with a halo and all haloes are 200 times the background density whatever their mass  $M$ . Sufficiently massive haloes typically host more than one galaxy. The halo model we use distinguishes between the central galaxy in a halo and the others, which are usually called satellites.

**Table 4.** Details of the HOD fits to the auto-correlation function for the full sample and the cross-correlation function for the matched and radio samples.

Selection	Density ( $10^{-4}h^3Mpc^{-3}$ )	$M_{\min}$ ( $10^{13}h^{-1}M_{\odot}$ )	$M_1$ ( $10^{13}h^{-1}M_{\odot}$ )	$\alpha$	$\chi^2_{red}$	$b_g$	$M_{\text{eff}}$ ( $10^{13}h^{-1}M_{\odot}$ )	$F_{\text{sat}}$ (%)
Full	$1.55 \pm 0.02$	$1.96 \pm 0.02$	$24.6 \pm 1.1$	$1.93 \pm 0.13$	1.2	$2.15 \pm 0.01$	$4.56 \pm 0.09$	$5.2 \pm 0.7$
Matched	$0.45 \pm 0.01$	$4.70 \pm 0.09$	$> 59.5$	$> 0.85$	1.0	$2.49 \pm 0.02$	$6.44 \pm 0.32$	$0.9 \pm 1.9$
Radio	$0.15 \pm 0.05$	$9.65 \pm 2.2$	$> 80.0$	$> 0.6$	0.82	$2.96 \pm 0.17$	$10.1 \pm 1.4$	$0.0 \pm 4$

**Figure 5.** The projected 2pt-auto-correlation function for the full LRG sample (stars) and the projected 2pt-cross-correlation function for the radio sample (open circles) and a sample randomly selected from the whole sample to match the luminosity, colour and  $z$  distributions of the radio sample (filled circles). The solid lines show the best fitting HODs on scales  $0.32 < r_p < 50h^{-1}$  Mpc. The dashed lines show the fit to the full sample, and the dotted line the fit achieved applying a power-law radio fraction to the matched HOD fit (see text for details).

The fraction of haloes of mass  $M$  which host centrals is modelled as

$$\langle N_c|M \rangle = \exp(-M_{\min}/M). \quad (5)$$

Only haloes which host a central may host satellites. In such haloes, the number of satellites is drawn from a Poisson distribution with mean

$$\langle N_s|M \rangle = (M/M_1)^\alpha. \quad (6)$$

Thus, the mean number of galaxies in haloes of mass  $M$  is

$$\langle N|M \rangle = \langle N_c|M \rangle [1 + \langle N_s|M \rangle], \quad (7)$$

and the predicted number density of galaxies is

$$n_g = \int dM n(M) \langle N|M \rangle, \quad (8)$$

where  $n(M)$  is the halo mass function, for which we use the parametrisation given by Sheth & Tormen (1999).

We further assume that the satellite galaxies in a halo trace an NFW profile (Navarro et al. 1996) around the halo centre, and that the haloes are biased tracers of the dark matter distribution. The halo bias depends on halo mass in a way that can be estimated directly from the halo mass function (Sheth & Tormen 1999). With these assump-

tions, the halo model for  $\xi(r)$  is completely specified (e.g. Cooray & Sheth 2002). Our model for the real space 2pt-auto-correlation function is given in detail in Wake et al. (2008), where the mean number density of central-satellite pairs within haloes of mass  $M$  is  $n(M) \langle N_c|M \rangle \langle N_s|M \rangle$ , and the mean number density of distinct satellite-satellite pairs is  $n(M) \langle N_c|M \rangle \langle N_s|M \rangle^2/2$ . In this work we use the 2pt-cross-correlation function, where we are cross-correlating a sub-sample of LRGs (either the radio-detected or matched samples) with the full sample of LRGs. We model the cross-correlation function in the halo model framework analogously to the auto-correlation function with the mean number density of central-satellite pairs,

$$n_{cs}(M) = n(M) \langle N_{c1}|M \rangle [\langle N_s|M \rangle + \langle N_{s1}|M \rangle], \quad (9)$$

and the mean number density of distinct satellite-satellite pairs,

$$n_{ss}(M) = n(M) \langle N_{c1}|M \rangle \langle N_s|M \rangle \langle N_{s1}|M \rangle, \quad (10)$$

where the pairs are between the full sample and sub-sample, and the terms with a subscript 1 are for the sub-sample and those without are for the full sample.

Since in our definition of the HOD a halo must contain a central if it is to contain a satellite, whether for the full sam-

ple or sub-sample, then only haloes that have a central in the sub-sample will contribute to the cross-correlation function. This is why only the fraction of haloes which contain a central of the sub-sample  $\langle N_{c1}|M \rangle$  appears in equations 9 and 10, not the equivalent fraction for the full sample  $\langle N_c|M \rangle$ .

Our model for the real-space 2pt-cross-correlation function is then

$$\xi_{12}(r) = 1 + \xi_{cs}(r) + 1 + \xi_{ss}(r) + \xi_{2h12}(r) \quad (11)$$

where

$$1 + \xi_{cs12}(r) = \int dM \frac{n_{cs12}(M)}{n_{g1}n_{g2}} \frac{\rho(r|M)}{M} \quad (12)$$

$$1 + \xi_{ss12}(r) = \int dM \frac{n_{ss12}(M)}{n_{g1}n_{g2}} \frac{\lambda(r|M)}{M^2} \quad (13)$$

and

$$\xi_{2h12}(r) = \int \frac{dk}{k} \frac{k^3 P_{2h12}(k)}{2\pi^2} \frac{\sin kr}{kr} \quad (14)$$

with

$$P_{2h12}(k) = b_{g1}(k)b_{g2}(k) P_{\text{Lin}}(k), \quad (15)$$

where

$$b_g(k) = \int dM \frac{n(M)}{n_g} b(M) \left[ \langle N_c|M \rangle + \langle N_s|M \rangle u(k|M) \right].$$

In the expressions above,  $\rho(r|M)$  is the density profile of haloes of mass  $M$ ,  $\lambda(r|M)$  denotes the convolution of two such profiles,  $u(k|M)$  is the Fourier transform of  $\rho(r|M)/M$ , and  $P_{\text{Lin}}(k)$  denotes the linear theory power spectrum. In practise, we approximate  $b_g(k)$  by its value  $b_g$  at  $k = 0$  (equation 16). All these quantities, along with the mass function  $n(m)$  and halo bias factor  $b(M)$ , are to be evaluated at the redshift of interest. We then calculate  $w(r_p)$  from  $\xi(r)$  using equation (3).

## 5.2 Application to the 2SLAQ LRG data

This model for the cross-correlation-function makes the assumption that the two galaxy samples occupy the same haloes, and that the satellite galaxies of both samples follow the same profile within the haloes. Whilst this is not necessarily valid for two independent galaxy samples, it should hold here as one sample is always a subset of the other.

This form of the halo model makes the explicit assumption of a volume-limited sample of galaxies. The 2SLAQ LRG sample as a whole is magnitude-limited rather than volume-limited, but (as may be seen from Table 4 of Sadler et al. 2007), the radio-detected LRGs are significantly brighter than the LRG sample as a whole. For this reason, Sadler et al. (2007) argue that the sample of radio-detected 2SLAQ LRGs is close to volume-limited, with no strong correlation between absolute magnitude (or radio luminosity) and redshift.

Nevertheless, since the use of a magnitude-limited sample may have the effect of biasing any derived quantities we may wish to measure from the HOD (such as the typical halo mass or satellite fraction) we carried out some further investigations. In the Appendix, we investigate the consequences of applying the halo model to magnitude-limited galaxy samples using the latest semi-analytic galaxy formation models (Font et al. 2008) applied to the Millennium

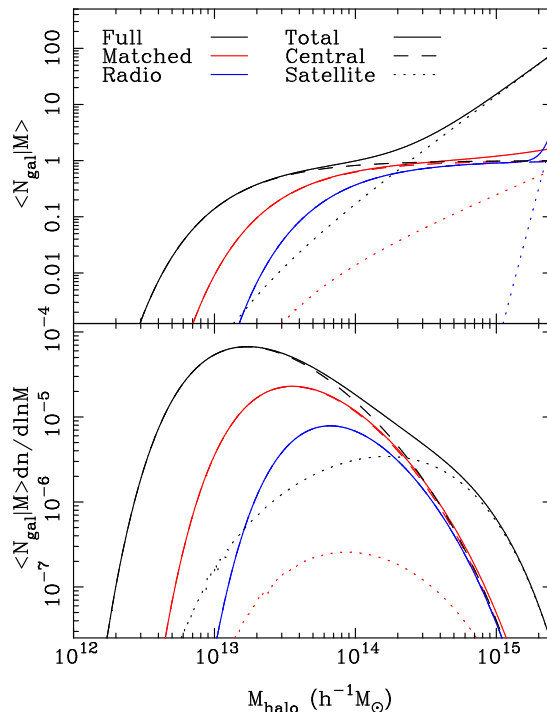


**Figure 6.** The mean number of LRGs per halo as a function of halo mass (top) and the mean number of LRGs per halo normalised by the number of haloes as a function of mass (bottom) for the best fitting HODs of the three samples. The full sample is shown by the black lines, the radio sample is shown by the blue lines and the luminosity, colour and redshift matched sample is shown by the red line. The total, central and satellite contributions are shown by the solid, dashed and dotted lines respectively. Whilst the spike at large halo masses in the radio HOD is the best fit, the HOD parameters describing the satellites are very poorly fit and a model with no satellites represents a better fit to the data.

simulation (Springel et al. 2005). We show that the halo model successfully recovers the effective halo mass to within 5% and so we are confident in applying this model to the 2SLAQ LRG samples.

We can now fit this model to the measured clustering and find the best fitting HOD parameters  $M_{\text{min}}$ ,  $M_1$ , and  $\alpha$ . We first make a  $\chi^2$  fit to the full LRG sample, fitting both the measured 2pt-auto-correlation function and the measured space density of  $1.55 \times 10^{-4} h^3 \text{Mpc}^{-3}$  as was done by Wake et al. (2008). We then use the resulting best fit HOD when fitting the cross-correlation function of the matched and radio samples. We note that including the density for the radio sample in this fitting process produces a poor fit to the clustering. This is not surprising, since only a small fraction (3–4%) of the 2SLAQ LRGs are detected as radio sources and so their overall space density is very low. Our HOD parametrisation assumes that all haloes above a certain mass contain at least one galaxy. Therefore the lower the galaxy density, the higher the typical mass and the higher the clustering. This is a good parametrisation for the whole galaxy population limited by optical luminosity, due to the correlation between central galaxy stellar mass and the halo mass. However, if the duty cycle of radio emission is such

that only a fraction of LRGs that could be radio loud actually show emission at a given time, then the measured space density of the radio-detected objects is a product of both the parent population space density and the fractional duty cycle.

To account for this, we could modify our HOD to include a term determining the fraction of LRGs which are currently radio-emitting. Initially we chose a simpler approach by not including the density and fitting the clustering alone. We can then compare the density predicted by the best-fitting HOD to the measured value and determine the fraction of LRGs with the same clustering as the radio sources which are currently radio-loud. By doing this, we are assuming that the relationship between halo mass and the probability of a galaxy having detectable radio emission takes the same form that we use to relate halo mass and luminosity, multiplied by some fraction which is independent of halo mass.

### 5.3 Results

Figure 5 shows the best fitting HODs for the three samples with the best-fitting parameters given in Table 4. We can use the HODs to calculate some other useful quantities such as the average linear bias ( $b_g$ ), the effective halo mass ( $M_{\text{eff}}$ ) and the satellite fraction ( $F_{\text{sat}}$ ), where

$$b_g = \int dM n(M) b(M) \langle N \rangle / n_g, \quad (16)$$

$$M_{\text{eff}} = \int dM M n(M) \langle N \rangle / n_g, \quad (17)$$

and

$$F_{\text{sat}} = \frac{\int dM n(M) \langle N_s | M \rangle}{\int dM n(M) \langle N | M \rangle}. \quad (18)$$

The values of these quantities for each sample are given in Table 4.

As we would expect from the relative clustering strength, we find a significantly higher minimum halo mass ( $M_{\text{min}}$ ) for the radio sample than the matched sample, confirming that the radio galaxies are typically found in more massive haloes. This is further confirmed by the calculated values of  $M_{\text{eff}}$  and  $b_g$ .

The parameters  $M_1$  and  $\alpha$  describing the satellite population are quite poorly constrained by these fits, with a large range of parameter space with high  $M_1$  or  $\alpha$  having a very similar  $\chi^2$ . This is because these samples have very low numbers of satellites, with the best fitting HODs for the matched and radio samples being consistent with having no satellite galaxies.

The best-fitting HODs are plotted in Figure 6, which shows the number of galaxies as a function of halo mass (top) and the number of galaxies weighted by the number of haloes as a function of halo mass (bottom). Each plot shows the total galaxy distributions, as well as those of the central and satellite galaxies independently. These plots clearly show that for both the radio-detected and matched samples, satellite galaxies are only present in the most massive haloes. Since there are so few haloes with these high masses, their total contribution is very low. This also explains why  $M_1$  and  $\alpha$  are given as  $1\sigma$  lower limits in Table 4. When

$M_1$  becomes significantly large there is essentially no contribution to the clustering from satellites since there are so few haloes at these masses, so the fit is equally as good for any large value of  $M_1$  or  $\alpha$ . In fact, fitting a model with no satellite galaxies produces a  $\chi^2$  only marginally higher for both the radio-detected and matched samples, and so gives significantly better fits overall because of the larger number of degrees of freedom in the model with satellites.

### 5.4 HOD models and the radio-galaxy duty cycle

We derive a space density  $0.15 \pm 0.05 \times 10^{-4} h^3 \text{Mpc}^{-3}$  for the best-fitting HOD to the radio-detected LRG sample. This can now be compared to the measured density of 2SLAQ LRGs which are currently detected as radio sources<sup>2</sup>,  $0.041 \pm 0.003 \times 10^{-4} h^3 \text{Mpc}^{-3}$ . Taking the ratio of these two numbers suggests that about 30% of all 2SLAQ LRGs with the same clustering properties as the radio-detected sample are currently radio-loud. This in turn implies a fairly high duty cycle for radio-loud AGN in the central galaxies of clusters at  $z \simeq 0.55$ , and is consistent with the radio detection rate of the brightest 2SLAQ LRGs ( $28 \pm 8\%$  for  $M_{0.2,r} < -23.75$  from Table 4 of Sadler et al. 2007).

The above discussion relies on our assumption that the form of the HOD for the radio-detected LRGs is the same as the standard form for a luminosity-limited sample. In that case the only mass-dependent probability of an LRG being radio-loud is determined by  $M_{\text{min}}$ , and there is then a halo mass-independent probability of  $\sim 30\%$  of a galaxy being currently powerful enough to be detected as a radio source at  $\gtrsim 10^{24} \text{W Hz}^{-1}$ . However it may be the case that the HOD for radio LRGs takes a different form from that given in equations 9 and 10, since one might expect it to consist of the standard form plus some term describing how the fraction of radio loud LRGs depends on halo mass ( $F_{\text{rad}}(M)$ ).

We can attempt to determine  $F_{\text{rad}}(M)$  by trying to modify the best fitting HOD to the matched sample in such a way that we reproduce the clustering and space density of the radio-detected LRG population. We chose to model  $F_{\text{rad}}(M)$  as a power law such that

$$F_{\text{rad}}(M) = f_r (M/M_{\text{rad}})^\beta, \quad (19)$$

where  $M_{\text{rad}} = 10^{14} h^{-1} M_\odot$  and  $F_{\text{rad}}(M) \leq 1$ .

Figure 7 shows the best fitting power law for  $F_{\text{rad}}(M)$ , HOD and space density distribution, along with the best fitting standard HOD given in Table 4. The fit to the clustering is shown as the dotted line in Figure 5. The best fit has a

<sup>2</sup> This value is found simply by dividing the total number of radio-detected LRGs by the survey completeness and co-moving volume between  $0.44 < z < 0.76$  in the 2SLAQ survey area. Our clustering analysis uses the full 2SLAQ LRG sample, which is magnitude-limited and so includes a smaller contribution from lower-luminosity galaxies than would be expected in a volume-limited sample. For this reason, we argue that the simple space density derived above is the appropriate one to use in this comparison. If we integrate over the radio luminosity function (RLF) in Table 5 of Sadler et al. (2007), which uses the  $V_{\text{max}}$  estimator to correct for the effects of the magnitude limit, we obtain a slightly higher value of  $0.067 \pm 0.004 \times 10^{-4} h^3 \text{Mpc}^{-3}$  for the volume-limited sample, which would increase the estimated radio-loud fraction from  $\sim 30\%$  to  $\sim 45\%$

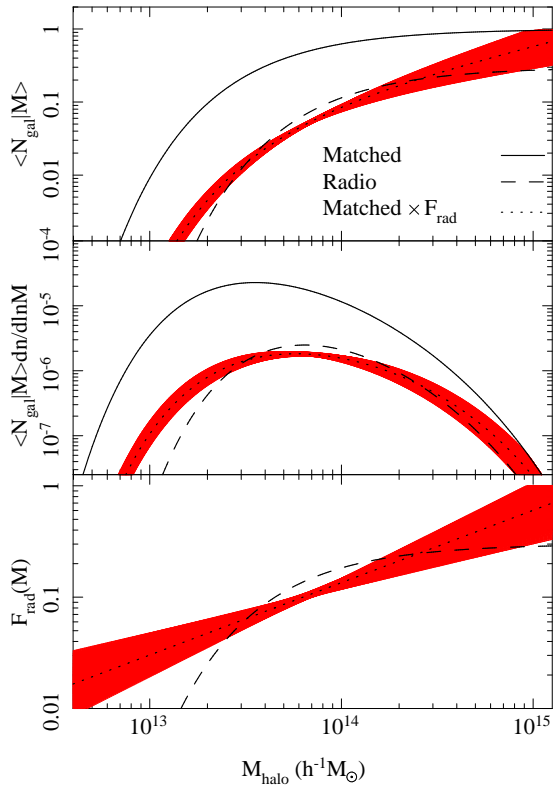


**Figure 7.** The mean number of LRGs per halo (top), the mean number of LRGs per halo normalised by the number of haloes (middle), the fraction of radio-loud LRGs (bottom), all as a function of halo mass. The solid line shows the best fit to the matched sample, the dashed line shows the best fit to the radio sample when the density is matched, and the dotted line shows the best fitting matched HOD plus power-law radio fraction to the radio clustering. The red area shows the  $1\sigma$  error on the dotted line.

slope  $\beta = 0.65 \pm 0.23$  and normalisation  $f_r = 0.14 \pm 0.02$ . The best fitting bias and effective halo mass are almost identical to those determined with the simple luminosity limit HOD, with  $b_g = 2.93 \pm 0.19$  and  $M_{eff} = 10.3 \pm 1.9 \times 10^{13} h^{-1} M_\odot$ . This is reassuring, since it implies that the determination of the typical halo mass is largely independent of the form of the HOD, providing that it yields a reasonable fit to the clustering and space density.

We also show in the bottom panel of Figure 7  $F_{rad}(M)$  determined by dividing the best-fitting luminosity limit HODs to the radio and matched samples (shown by the blue and red lines in Figure 6). While both HOD fits, with and without the power law, provide good statistical fits to our data, they diverge for halo masses above  $10^{15} h^{-1} M_\odot$  (where the power-law fit suggests that  $\sim 60\%$  of central cluster galaxies would be radio-loud, while the luminosity-limit HOD suggests that the fraction levels off at  $\sim 30\%$ ) and below a few times  $10^{13} h^{-1} M_\odot$  (where the luminosity-limit HOD suggests that there should be a sharp cut off in the fraction of radio-loud LRGs). Since the current 2SLAQ LRG data sample contains very few objects with halo masses above  $10^{15} h^{-1} M_\odot$  or below  $3 \times 10^{13} h^{-1} M_\odot$ , a larger sample of radio galaxies is needed to test between different models in this regime.

**Table 5.** Radio-detected fraction of brightest-cluster galaxies (above a limiting 1.4 GHz radio power  $P_{1.4}$ ) in the local universe and at  $z \sim 0.55$ .

Sample	$P_{1.4}$ ( $\text{W Hz}^{-1}$ )		Reference
	$\geq 10^{23}$	$\geq 10^{24}$	
BCGs, $z < 0.11$	33.3%	22.2%	Burns 1990
BCGs, $z < 0.2$	32.7%	19.9%	Lin & Mohr 2007
BCGs, SDSS	$\sim 30\%$	$\sim 20\%$	Best et al. 2007
2SLAQ LRGs	...	$> 30\%$	This paper

## 6 DISCUSSION AND CONCLUSIONS

We have measured the two-point cross-correlation function of a sample of radio-detected LRGs at  $z \simeq 0.55$  and a sample of radio-quiet LRGs that matches the luminosity, colour and redshift distribution of the radio loud sample. We find that radio-detected LRGs at  $z \simeq 0.55$  are significantly more clustered than the matched radio-quiet sample, with clustering scale lengths ( $r_0$ ) of  $12.3 \pm 1.2$  and  $9.02 \pm 0.52 h^{-1}$  Mpc respectively. This result suggests that the radio-detected LRGs typically occupy more massive haloes than other LRGs of the same optical luminosity and stellar mass. We confirm this by fitting HODs to the observed clustering, and show that the radio-detected LRGs have a typical halo mass of  $10.1 \pm 1.4 \times 10^{13} h^{-1} M_\odot$  and a bias of  $2.96 \pm 0.17$ , compared to a halo mass of  $6.44 \pm 0.32 \times 10^{13} h^{-1} M_\odot$  and a bias of  $2.49 \pm 0.02$  for the radio-quiet LRGs.

The clustering of the radio-detected LRGs is best fitted by a HOD containing only galaxies which occupy the centres of haloes and are not satellites, though the current data do not allow us to exclude models with some radio satellite galaxies. We show that the dependence on radio fraction on halo mass can be modelled as a power-law with slope  $0.65 \pm 0.23$ , although it will take a larger samples of radio galaxies with a more precise clustering measurement to rule out other forms of this dependence. Such samples are available at lower redshift, such as the SDSS/NVSS/FIRST sample presented by Best et al. (2005), which would also allow a measurement of any evolution in this relationship. Mandelbaum et al. (2008) use both a clustering and weak lensing analysis of this sample to show that the the halo masses of radio loud galaxies are about twice the mass of a comparable radio quiet sample, in good agreement with the results presented here.

Table 5 compares the radio detection rates for the most optically-luminous brightest cluster galaxies (BCGs) in the local universe with the 2SLAQ LRG value derived in §5.4. The values found in the three local studies are remarkably consistent, and imply that the radio power above which at least 30% of BCGs are detected rises from about  $10^{23} \text{ W Hz}^{-1}$  at  $z \sim 0.1$  to at least  $10^{24} \text{ W Hz}^{-1}$  at  $z \sim 0.55$ .

As noted by Johnston et al. (2008) low-power ( $< 10^{26} \text{ W Hz}^{-1}$ ) radio galaxies in the 2SLAQ LRG sample have stellar populations which are generally no different from those in a radio-quiet comparison sample, and the majority of these radio galaxies have weak or no emission lines in their optical spectra. These properties are consistent with a population of ‘low-excitation’ radio galaxies powered by Bondi accretion of hot, X-ray emitting gas from the intergalactic medium (Allen et al. 2006; Hardcastle, Evans &

Croston 2007). If this is correct, then the highly-clustered environment of the 2SLAQ radio galaxies is not surprising. The radio emission from central cluster galaxies could be enhanced by the presence of a denser intracluster medium (ICM) which would both confine the radio lobes and provide a more efficient working surface for the radio jets, thus boosting the observed radio luminosity (Barthel & Arnaud 1996; Allen et al. 2006). However, Best et al. (2006) argue that this boosting of radio emission from cluster galaxies only applies to powerful radio sources which extend well beyond the host galaxy and into the intracluster medium. Since most of the radio-detected 2SLAQ LRGs are low-power radio galaxies whose radio emission is generally compact and confined within the host galaxy, this ICM-related boosting may not play a strong role.

The most likely alternative is that the radio emission from central cluster galaxies is boosted because of a higher fuelling rate of gas onto the central black hole. This is plausible because gas from both the galaxy's own X-ray halo and a larger-scale cluster cooling flow can contribute to the fuelling of an active nucleus in central cluster galaxies (Best et al. 2007).

## ACKNOWLEDGEMENTS

We acknowledge the support of the Australian Research Council through the award of an ARC Australian Professorial Fellowship to EMS and a QEII Fellowship to SMC. This work was also supported in part by a rolling grant from the UK STFC.

The authors would like to thank Ravi Sheth for assistance with implementing the cross-correlation function calculation in the halo model, and Richard Bower, Shaun Cole, Russell Smith and the anonymous referee for helpful discussions and insightful comments on this work. The authors thank the 2SLAQ team and the AAO staff for their contributions to the collection of the 2SLAQ data (<http://www.2slaq.info/>). DAW thanks the Department of Astronomy at the University of Illinois for their regular hospitality.

We would like to thank Cameron McBride, Jeff Gardner, and Andy Connolly for providing a pre-release version of the Ntropy package. Ntropy was funded by the NASA Advanced Information Systems Research Program grant NNG05GA60G.

Funding for the SDSS and SDSS-II has been provided by the Alfred P. Sloan Foundation, the Participating Institutions, the National Science Foundation, the U.S. Department of Energy, the National Aeronautics and Space Administration, the Japanese Monbukagakusho, the Max Planck Society, and the Higher Education Funding Council for England. The SDSS Web Site is <http://www.sdss.org/>.

The SDSS is managed by the Astrophysical Research Consortium for the Participating Institutions. The Participating Institutions are the American Museum of Natural History, Astrophysical Institute Potsdam, University of Basel, Cambridge University, Case Western Reserve University, University of Chicago, Drexel University, Fermilab, the Institute for Advanced Study, the Japan Participation Group, Johns Hopkins University, the Joint Institute for Nuclear Astrophysics, the Kavli Institute for Particle As-

trophysics and Cosmology, the Korean Scientist Group, the Chinese Academy of Sciences (LAMOST), Los Alamos National Laboratory, the Max-Planck-Institute for Astronomy (MPIA), the Max-Planck-Institute for Astrophysics (MPA), New Mexico State University, Ohio State University, University of Pittsburgh, University of Portsmouth, Princeton University, the United States Naval Observatory, and the University of Washington.

## REFERENCES

- Allen, S.W., Dunn, R.J.H., Fabian, A.C., Taylor, G.B., Reynolds, C.S., 2006, MNRAS, 372, 21
- Auriemma, C., Perola, G.C., Ekers, R.D., Fanti, R., Lari, C., Jaffe, W.J., Ulrich, M.H., 1977, A&A, 57, 41
- Barthel, P., Arnaud, K., 1996, MNRAS, 284, L45
- Becker, R.H., White, R.L., Helfand, D.J., 1995, ApJ, 450, 559
- Berlind A. A., Weinberg D. H., 2002, ApJ, 575, 587
- Best, P.N., Kauffmann, G., Heckman, T., Brinchmann, J., Charlot, S., Ivezić, Z., White, S.D.M., 2005a, MNRAS 362, 25
- Best, P.N., Kauffmann, G., Heckman, T., Ivezić, Z., 2005b, MNRAS 362, 9
- Best, P.N., Kaiser, C.R., Heckman, T.M., Kauffmann, G., 2006, MNRAS, 368, L67
- Best, P.N., von der Linden, A., Kauffmann, G., Heckman, T.M., Kaiser, C.R., 2007, MNRAS, 374, 908
- Blake, C., Wall, J., 2002, MNRAS, 337, 993
- Blake, C., Mauch, T., Sadler, E., 2004, MNRAS, 347, 787
- Bock, D. C.-J., Large, M. I., Sadler, E.M., 1999, AJ, 117, 1578
- Bower R. G., Benson A. J., Malbon R., Helly J. C., Frenk C. S., Baugh C. M., Cole S., Lacey C. G., 2006, MNRAS, 370, 645
- Cannon, R.D. et al., 2006, MNRAS, 372, 425
- Ciotti L., Ostriker J. P., 2007, ApJ, 665, 1038
- Colless, M. et al., 2001, MNRAS, 328, 1039
- Condon, J.J., Cotton, W.D., Greisen, E.W., Yin, Q.F., Perley, R.A., Taylor, G.B., Broderick, J.J., 1998, AJ, 115, 1693
- Cooray A., Sheth R., 2002, PhR, 372, 1
- Croton D. J., et al., 2006, MNRAS, 365, 11
- Davis M., Peebles P. J. E., 1983, ApJ, 267, 465
- Fanaroff, B.L., Riley, J.M., 1974, MNRAS, 167, 31
- Font A. S., et al., 2008, MNRAS, 389, 1619
- Gardner, J. P., Connolly, A., & McBride, C. 2007, ArXiv e-prints, 709, arXiv:0709.1967
- Hardcastle, M.J., Evans, D.A., Croston, J.H., 2007, MNRAS, 376, 1849
- Heckman, T.M., Smith, E.P., Baum, S.A., van Breugel, W.J.M., Miley, G.K., Illingworth, G.D., Bothun, G.D., Balick, B., 1986, ApJ, 311, 526
- Jing Y. P., Mo H. J., Boerner G., 1998, ApJ, 494, 1
- Johnston, H.M., Sadler, E.M., Cannon, R., Croom, S.M., Ross, N.P., Schneider, D.P., 2008, MNRAS, 384, 692
- Ledlow, M.J., Owen, F.R., 1996, AJ, 112, 9
- Ma C.-P., Fry J. N., 2000, ApJ, 543, 503
- Mandelbaum R., Li C., Kauffmann G., White S. D. M., 2008, arXiv, arXiv:0806.4089
- Mauch, T., Sadler, E.M., 2007, MNRAS, 375, 931

- Navarro, J. F., Frenk, C. S., & White, S. D. M. 1996, ApJ, 462, 563
- Overzier, R. A., Röttgering, H.J.A., Rengelink, R.B., Wilman, R.J., 2003, A&A, 405, 530
- Parma P., Murgia M., Morganti R., Capetti A., de Ruiter H. R., Fanti R., 1999, A&A, 344, 7
- Peacock J. A., Smith R. E., 2000, MNRAS, 318, 1144
- Prestage, R.M., Peacock, J.A., 1988, MNRAS, 230, 131
- Sadler, E.M. et al., 2007, MNRAS, 381, 211
- Scoccimarro R., Sheth R. K., Hui L., Jain B., 2001, ApJ, 546, 20
- Scranton, R., et al. 2002, ApJ, 579, 48
- Seljak U., 2000, MNRAS, 318, 203
- Sheth, R. K., & Tormen, G. 1999, MNRAS, 308, 119
- Springel V., et al., 2005, Natur, 435, 629
- Wake D. A., et al., 2006, MNRAS, 372, 537
- Wake D. A., et al., 2008, MNRAS, 387, 1045
- York, D.G. et al., 2000, AJ 120, 1579
- Zehavi, I., et al. 2005, ApJ, 621, 22

## APPENDIX A: FITTING THE HALO MODEL TO A MAGNITUDE LIMITED SAMPLE

In section 5 we estimate the bias and effective halo mass of effectively magnitude-limited galaxy samples using the halo model framework. The halo occupation distribution we use is designed to apply to volume limited galaxy samples and so its application here may result in biased estimates of these parameters. In this appendix we use the millennium simulation to investigate the magnitude of this bias and show that it is likely to be only  $\sim 5\%$ , and comparable to the likely systematic error introduced by any differences between the assumed form of the HOD and the actual form.

We construct two samples of galaxies generated using the latest version of the Durham group semi-analytic galaxy formation model detailed in Font et al. (2008). For the first sample we simply select all galaxies in the  $z = 0.02$  volume with SDSS  $r$  magnitudes  $< -22$  i.e. a volume limited sample of galaxies with a space density equivalent to our full LRG sample. We also wish to generate a magnitude limited sample, and so calculate the apparent SDSS  $r$  magnitude of each galaxy in our volume assuming an observer at one edge of that volume. We then limit this sample to  $r < 19.67$  which matches the space density of the volume limited sample. Both samples contain  $\sim 20,000$  galaxies. Fig. A1 shows the absolute magnitude distribution and real space 2pt-auto correlation function for these samples. As one would expect the magnitude limited sample which contains some intrinsically fainter galaxies shows a slightly lower clustering amplitude. In order to test whether we are able to accurately measure the effective halo mass by fitting a HOD to the clustering measurements we first determine the actual HOD of the two galaxy samples shown as the solid lines in Fig. A2. We then take a suitable analytic form of the HOD and fit it to both the actual HOD from the simulation and the derived 2pt-correlation function and space density, shown as the dashed and dotted lines respectively. It is worth noting that the actual HOD derived from GALFORM does not exactly match our analytic form at low masses and would not match any form typically used in the literature. The clear 'bump' at

**Table A1.** The Effective halo mass in units of  $10^{13}h^{-1}M_{\odot}$ .

Method	Volume Limited	Magnitude Limited
Actual	6.63	6.38
HOD fit	$6.98 \pm 0.09$	$6.87 \pm 0.08$
Clustering fit	$7.01 \pm 0.11$	$6.78 \pm 0.11$

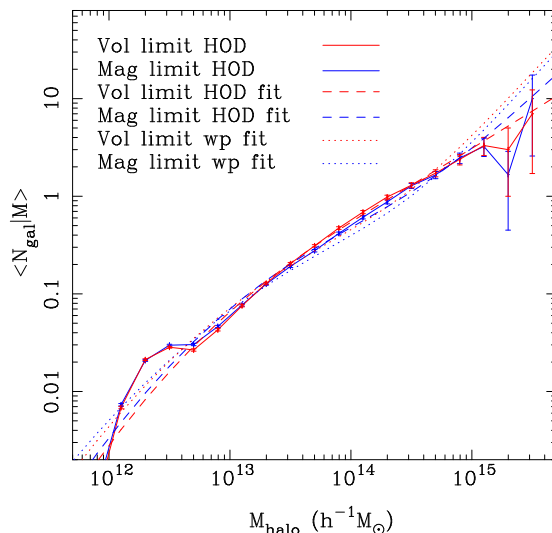


**Figure A2.** The measured HOD for the volume (red) and magnitude (blue) limited samples, as well as analytic HOD fits to the measured HODs (dashed lines) and the clustering (dotted lines).

$10^{12} < M_{\text{halo}} < 10^{13}$  is caused by the onset of AGN feedback in model (Carlton Baugh, Private Communication). It will be interesting to see if there is any evidence for this in directly determined HODs of massive galaxies.

Despite the differences in the analytic and actual HODs the analytic HOD does provide good fits to the clustering and space density of the samples within the errors. Table A1 gives the values  $M_{\text{eff}}$  determined from fitting the analytic HOD to the measured HOD and the clustering as well as that determined directly from the simulation.  $M_{\text{eff}}$  is overestimated by  $\sim 7\%$  fitting the analytic form to either measured HOD or clustering for both the volume and magnitude limited samples, due to the excess of galaxies in the 'bump' in the HOD at low halo masses. The difference between the fits to the HOD and the clustering is larger for the magnitude-limited sample, but is still only at the 2% level and is consistent with the error on the fit to the clustering. We can therefore be confident that the likely magnitude of any systematic error on  $M_{\text{eff}}$  caused by fitting the HOD to a magnitude limited rather than volume-limited sample is less than the measurement errors for all the samples considered in Section 5. It is interesting to note that a larger systematic error in  $M_{\text{eff}}$  would be introduced if the true HOD is not well represented by the assumed analytic form of the HOD. However, one would expect still relative measurements of  $M_{\text{eff}}$  to be representative even in this case.

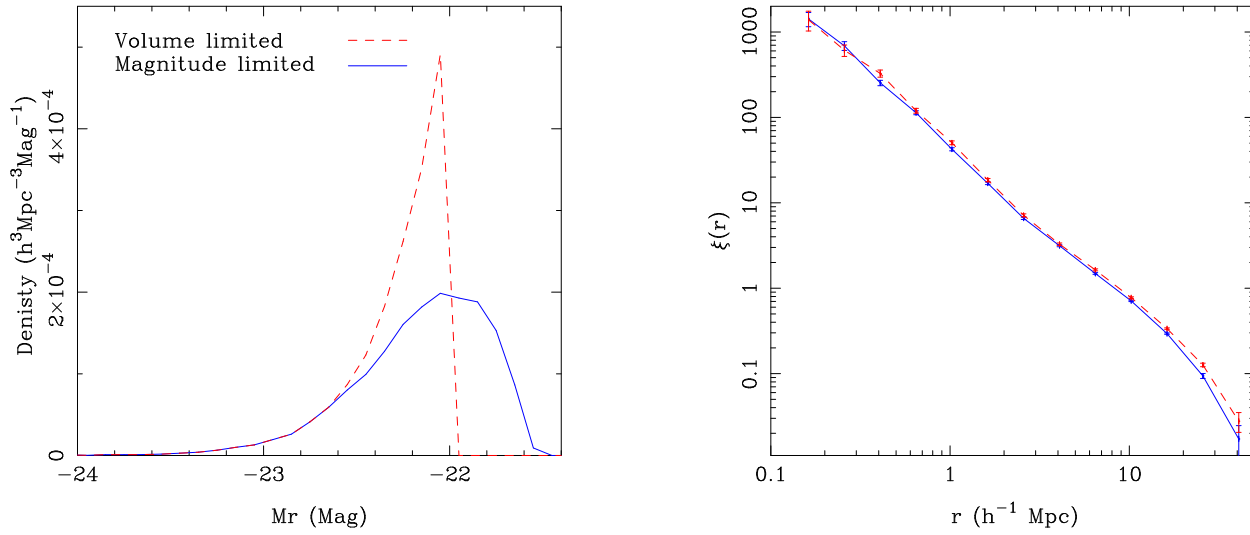


**Figure A1.** The absolute magnitude distribution (left) and the real space 2pt-correlation function (right) for the volume limited (dashed line) and magnitude-limited (solid line) simulated galaxy samples.

This paper has been typeset from a  $\text{T}_{\text{E}}\text{X}/\text{L}^{\text{A}}\text{T}_{\text{E}}\text{X}$  file prepared by the author.